



Ultrastable Crystalline Semiconducting Hydrogenated Borophene

Chuang Hou, Guoan Tai,* Jinqian Hao, Lihang Sheng, Bo Liu, and Zitong Wu

Abstract: Borophene sheets have been synthesized in recent experiments, but the metallic nature and structural instability of the sheets seriously prevent emerging applications. Hydrogenated borophene has been predicted as an ideal material for nanoelectronic applications due to its high stability as well as excellent electronic and mechanical properties. However, the fabrication of hydrogenated borophene is still a great challenge. Here, we demonstrate that hydrogenated borophenes in large quantities can be prepared without any metal substrates by a stepwise in-situ thermal decomposition of sodium borohydride under hydrogen as the carrier gas. The borophenes with good crystallinity exhibit superior stability in strong acid or base solvents. The structure of the grown borophene is in good agreement with the predicted semiconducting α -boron sheet. A fabricated borophene-based memory device shows a high ON/OFF-current ratio of 3×10^3 and a low operating voltage of less than 0.35 V as well as good stability.

Borophene was proposed after the planar hexagonal B_{36} cluster was found by combining computational studies and experimental observations.^[1a] The planar boron clusters and multicenter bonding found in the two-dimensional (2D) boron clusters are regarded as precursors to that in borophene.^[1] Inspired by these studies, borophene has drawn tremendous attention due to its unique physical and chemical properties, such as highly anisotropic electronic structure, mechanical compliance, ultrahigh thermal conductance, optical transparency, and phonon-mediated superconductivity.^[2–6] Owing to these excellent properties, borophene shows potential applications in nanoelectronics, optoelectronics, as well as energy storage and conversion.^[5] Borophene cannot be produced via exfoliation methods because it does not have a layered bulk counterpart, which originates from its severe electron deficiency with a diversity of bonds, which range from covalent two-center–two-electron (2c–2e) bonds up to multicenter bonds.^[5b,c,6b] The multicenter characteristics of boron bonds give rise to the formation of configurationally various synthetic 2D boron sheets, and the stability of borophene depends on the hexagon-vacancy concentration on metal substrates in the range of 1/6–1/9.^[7] Several 2D boron phases have been investigated, including honeycomb



and triangular borophene, α , β_{12} , δ_6 , and χ_3 boron sheets, and others.^[2,3,5b,7–9] Despite the considerable theoretical achievements, only very recently, a few types of boron sheets have been grown by the deposition of boron atoms on Ag(111),^[2,3] Cu(111),^[8] and Au(111)^[9] substrates under ultra-high vacuum conditions, and synthesized on Cu foils by chemical vapor deposition (CVD).^[4] However, the boron sheets are mostly unstable under air.^[2,3,5b,8,9] Additionally, the metallic character of boron sheets also seriously limits its potential applications in electronic devices.^[5] Therefore, the preparation of stable semiconducting boron sheets is a prerequisite for the application of borophene in high-performance nanoelectronics and optoelectronics.

Hydrogenation was predicted to be an effective strategy to stabilize the structure and open the band gap of 2D materials.^[10] For example, hydrogenation can convert graphene, silicene, and germanene from a good conductor to a semiconductor with a large band gap.^[10] Similarly, theoretical calculations show that hydrogenation is an effective approach to stabilize the structure of boron sheets and tune their electronic properties.^[11,12] Complete hydrogenation of borophene leads to the formation of borophane with remarkable stability.^[12] Furthermore, many unique physical properties of hydrogenated borophene have been predicted, such as a direction-dependent Dirac cone, an ultrahigh Fermi velocity four times higher than that of graphene, an excellent Young's modulus close to steel, an anisotropic quantum thermal conductance, and an outstanding Li- as well as Na-ion-storage capacity.^[5,11,12] The boron hydride layers also have the potential to form a three-center–two-electron (3c–2e) bond to stabilize the B–H sheet, which is important to explain the formation mechanism of organic boron hydride molecules, which lead to the Nobel prize in chemistry for William Nunn Lipscomb in 1976.^[13] Motivated by these achievements, the potentially stable inorganic boron hydrides have attracted timely interest. Hydrogen boride sheets derived from MgB_2 have been synthesized using the cation-exchange approach, but they are amorphous, which limits potential applications in electronic devices.^[14] Therefore, the development of stable and crystalline semiconducting hydrogenated borophene is of high importance for their practical applications.

We have successfully prepared large-scale hydrogenated borophenes in a hydrogen-rich environment. Under controllable conditions, we developed a three-step heating procedure by in-situ thermal decomposition of sodium borohydride ($NaBH_4$) to grow borophenes without any metal substrates. The morphologies and crystal structures of the borophenes were characterized by scanning electron microscopy (SEM), atomic force microscopy (AFM), high-resolution transmission electron microscopy (HRTEM), and selected-area electron diffraction (SAED). Their optical properties were tested by Raman, UV/Vis absorption, and photoluminescence (PL)

[*] C. Hou, Prof. G. Tai, J. Q. Hao, L. H. Sheng, B. Liu, Z. T. Wu

The State Key Laboratory of Mechanics and Control of Mechanical Structures and Laboratory of Intelligent Nano Materials and Devices of Ministry of Education, College of Aerospace Engineering, Nanjing University of Aeronautics and Astronautics
Nanjing 210016 (China)
E-mail: taiguaoan@nuaa.edu.cn

 Supporting information and the ORCID identification number(s) for the author(s) of this article can be found under:
 <https://doi.org/10.1002/anie.202001045>.

spectroscopy. Furthermore, their chemical compositions were determined by inductively coupled plasma (ICP) and organic elemental analysis. As a proof-of-concept application, a borophene-based non-volatile re-writable memory was fabricated with borophene as the charge-trapping material and polyvinylpyrrolidone as an insulator.

The experimental setup is schematically illustrated in Figure S1 a (Supporting Information). We developed a three-step heating process to synthesize large-scale and free-standing hydrogenated borophenes by in-situ thermal decomposition of NaBH_4 powders, as illustrated in Figure 1 a. The programmed temperature curve is shown in Figure S1 b. First, the powders were heated from room temperature to 490°C at a rate of 10°Cmin^{-1} and kept for 2 h to make them form an initial intermediate (Step I). Second, the intermediate was further heated to 550°C at a rate of 5°Cmin^{-1} and kept for 30 min to make them form a more stable intermediate (Step II). Third, the intermediate was ramped to 600°C at a rate of 5°Cmin^{-1} and kept for 30 min to produce large-scale borophenes (Step III). The corresponding SEM images of NaBH_4 , the intermediates, and the borophenes are shown in Figure 1 b–d. The results clearly show that the borophenes were synthesized by in-situ thermal decomposition of NaBH_4 under the programmed temperature procedure. The formation of crystalline borophenes is self-catalyzed by self-decomposing sodium atoms or clusters. The detailed principle will be discussed later.

A high-magnification SEM image (Figure 2 a) shows that the thickness of the borophenes can be down to less than 1 nm. It also shows that the lateral size of the sheets varies from 1 to $15\ \mu\text{m}$ and the average lateral size is around $5.14\ \mu\text{m}$ (Figure 2 b). AFM was employed to characterize the thickness and lateral size of the sheets further. The results show that the thickness of a typical sheet is close to 0.78 nm (Figure 2 c), the thickness distribution varies from 0.78 to 3.50 nm and the average thickness is around 1.8 nm (Figure S2 a–c). The X-ray

diffraction pattern of borophene is shown in Figure S2 d. A typical TEM image shows that the sheet, which has a lateral size of over $10\ \mu\text{m}$, is covering the holes of the TEM grid, and has a rolled-up edge (Figures 2 d and S2 e–i). A HRTEM image and the corresponding SAED pattern confirmed that this borophene is a single crystal. A HRTEM image extracted from the red rectangular region in Figure 2 e was reconstructed by masking the 2D fast-Fourier-transform (FFT) pattern (Figure 2 f), and the reconstructed image displays the structure of borophene with lattice spacings of approximately 4.31 and $4.36\ \text{\AA}$.

Furthermore, we performed first-principles calculations based on density functional theory (DFT) to search for the most probable structure of the boron sheets. Among the theoretically possible structures, we found that an α' -boron sheet bonded by 4 hydrogen atoms (α' -4H-borophene) with a vacancy concentration of 1/9 matches the experimental result.^[7a,15] To modulate the semiconductor characteristics of borophene, the adsorption sites of hydrogen atoms on borophene were optimized (Figures 2 g and S3). The lattice of α' -4H-borophene remains after ideal hydrogenation and the structure only exhibits a buckled configuration. The optimized structural parameters are listed in Table S1. Additionally, the chemical composition of the obtained borophene was confirmed by ICP as an ion source for mass spectrometry and an organic elemental analyzer. The elemental ratio of boron and hydrogen is around 2:1, which is close to that of the predicted α' -4H-borophene (B_8H_4), as shown in Table S2. The theoretical prediction is in good agreement with the experimental results (Figure 2 g–i).

The chemical bonding of α' -4H-borophene was investigated by X-ray photoelectron spectroscopy (XPS), as shown in Figure S4. The high-resolution B 1s spectrum is shown in Figure 3 a and features characteristic peaks located at 187.6 and $188.2\ \text{eV}$ in the range reported for bulk boron,^[3,4,16] indicating that there are two types of bonding structures with different chemical environments. To confirm the accuracy of the analysis of the B 1s spectrum, the C 1s spectrum of borophene was calibrated to $284.8\ \text{eV}$ (Figure 3 b). After exposure to air for more than two months, the sheets still preserved their structural integrity (Figure S5). To further confirm the stability of the sheets, we dispersed them into solutions of sodium hydroxide, ammonium thiosulfate, hydrochloric acid, and hydrofluoric acid in a concentration of $1\ \text{molL}^{-1}$ for 48 h, and centrifuged the solution to extract the sheets for XPS characterization (Figure S6). The experimental results clearly demonstrate that the XPS spectra of the sheets after the treatment are consistent with those of the original sample, suggesting that the

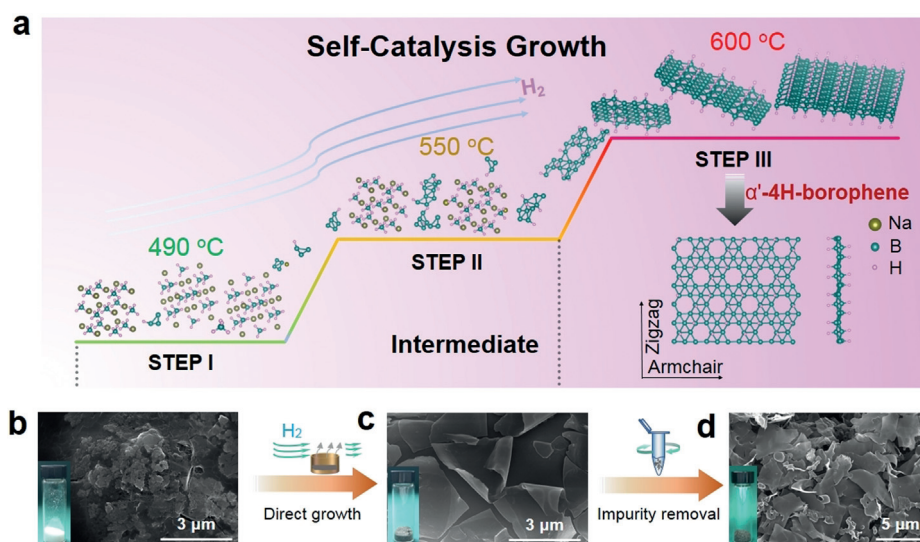


Figure 1. a) Schematic diagram of the in-situ and stepwise thermal decomposition of NaBH_4 . b)–d) SEM images of NaBH_4 (b) and hydrogenated borophene before (c) and after cleaning (d). The insets in (b–d) show corresponding photographs.

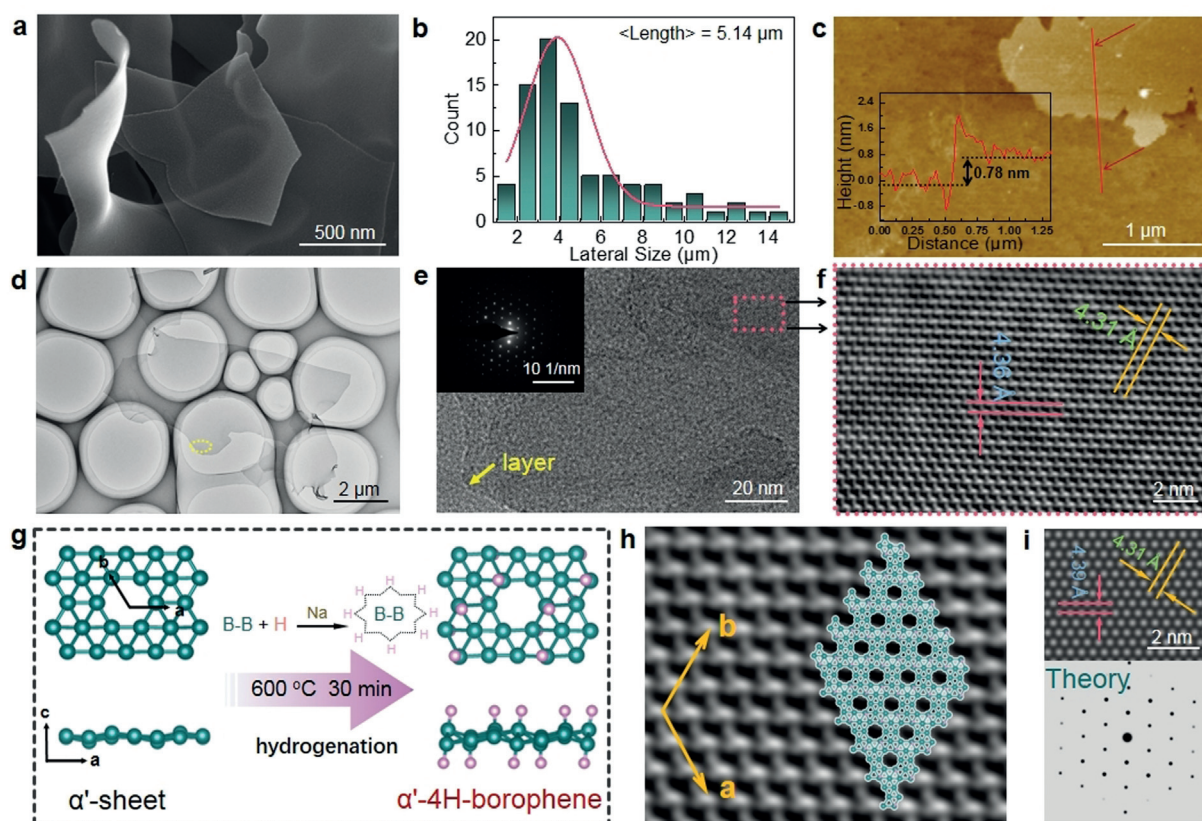


Figure 2. a) SEM image of the sheets. b) Statistical data of the lateral sizes of 80 sheets measured via SEM. c) AFM image of the sheet. Height analysis along the red line in the inset indicates a thickness of around 0.78 nm. d) Low-resolution TEM image of the sheet. e) HRTEM image of the sheet. The corresponding SAED image is shown in the inset. f) HRTEM image by masking the FFT pattern extracted from the red rectangular region in (e). g) Structure of the sheet. Two oppositely charged sublattices are indicated by different colors (B: dark cyan; H: pink). h) Experimental HRTEM images. i) Corresponding HRTEM map and SAED image extracted from the calculation model.

sheets are ultrastable owing to the surface hydrogenation. Moreover, the results also indicate that borophenes have a potential for application in high-performance devices in extreme environments.

The implementation of hydrogen into borophene was detected by time-of-flight secondary-ion mass spectrometry (TOF-SIMS), as shown in Figure S7a. Attenuated total-reflectance Fourier-transform infrared (ATR-FTIR) spectra were used to determine the structural characteristics of the sheets (blue) and bulk boron (green), as shown in Figure S7b. Unlike bulk boron, the absorption peaks of the sheets located at 1116 and 2485 cm^{-1} originate from the B–H stretching vibration of the 3c–2e bonds of borophene.^[17] Additionally, the B–B absorption peaks located at 1064, 1184, and 2889 cm^{-1} were observed in both borophene and bulk boron.^[17] The results further confirm that the borophenes were in-situ hydrogenated during the growth procedure.

Raman spectroscopy was employed to reveal the remarkable structure and unusual electronic as well as phonon properties of borophene (Figure 3c). The results show that the two intense peaks at 743 and 2500 cm^{-1} can be ascribed to the modes of the B–B cluster (E_g) and B–H bonds, respectively. The E_g mode is a mixture of two vibration modes of the B–B cluster^[18] with frequencies ω_1 and ω_2 . For ω_1 , all six external two-center bonds of the icosahedra are

compressed simultaneously.^[16] For ω_2 , two of the six are compressed, two are stretched and two are unstrained.^[16] The peak at 2500 cm^{-1} originates from the B–H stretching vibration, indicating the existence of terminal hydrogen atoms in borophene.^[19] Additionally, a peak located at 1065 cm^{-1} can be ascribed to $A_{1g} + E_g$ modes of the B–B clusters, which are attributed to either a B–H rocking mode or a B–H deformation.^[20] The Raman spectrum of the borophenes is completely different from those of NaBH_4 and boron oxide (Figure S7c,d).

To confirm the thermal stability, the sheets were annealed in a nitrogen-filled glove box and under air. No obvious Raman shift was observed even under air at temperatures of up to 400 °C (Figure S8), suggesting a superior stability of α' -4H-borophene, significantly higher than that reported for MoS_2 and other two-dimensional materials.^[21] Thermogravimetric analysis further shows the ultrastability of the sheets due to the absence of significant mass loss (Figure S9a). Therefore, the results let us conclude that the borophenes are ultrastable, and this work opens a door to realize the practical application of borophene devices under air and even at high temperatures.

To investigate the stability of α' -4H-borophene theoretically, the bonding energy of the H atom on the borophenes was calculated (Table S1 and Figure S10). Different bonding

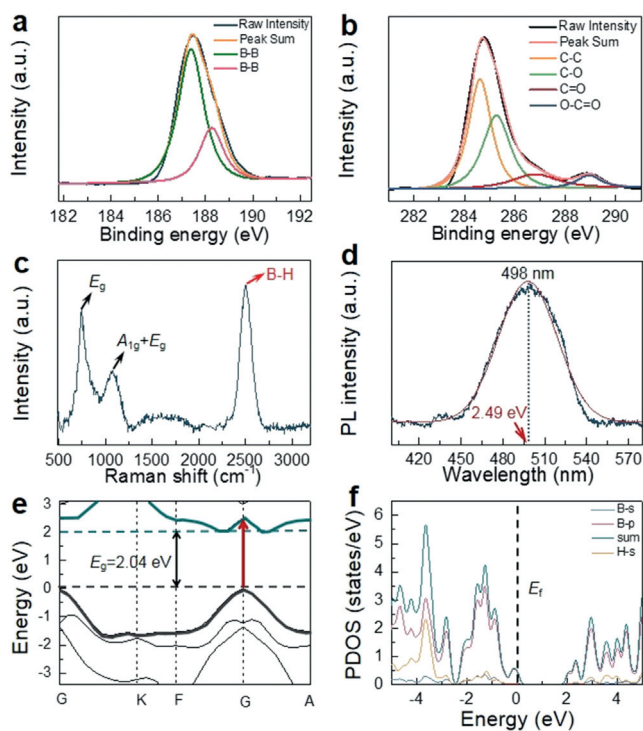


Figure 3. a) B 1s XPS spectrum of the sheets. b) High-resolution C 1s spectra of the sheets. c) Raman spectrum of the sheets. d) Photoluminescence spectrum of the sheets. The red line is a Gaussian fit. e) Electronic band structure of the sheet. The Fermi level is indicated by the black dashed line. f) Calculated total density of states (DOS, dark cyan line) and local DOS for the B-s (Cambridge blue line), B-p (pink line) and H-s (orange line) orbitals. The energies are given with respect to the valence-band maximum (VBM).

sites of the H atoms on the borophenes were considered, as shown in Figure S3. From the calculated band structure and density of states (DOS) based on the PBE functional, most of borophenes with a negative bonding energy (ΔE_b) are metallic except for α' -4H-borophene and α -4H-borophene with a B_8H_4 structure (Figures S11, S12). Although the structure of α -4H-borophene is very close to that of α' -4H-borophene, α' -4H-borophene, which has the lowest ΔE_b among the predicted structures, is well in accordance with the experimental results (Figure S10).

To examine the dynamic stability of α' -4H-borophene, the lattice dynamics was studied by calculating its phonon dispersion using a linear-response method within the DFT framework. The absence of imaginary modes in the whole Brillouin zone shows that α' -4H-borophene is stable (Figure S10b). Furthermore, the thermal stability of α' -4H-borophene was verified by performing an ab-initio molecular dynamics (AIMD) simulation at 700 K. The negligible buckling vibration was observed in α' -4H-borophene (Figure S13). Thus, α' -4H-borophene shows strong thermal and dynamic stability.

The optical properties of the borophenes were analyzed by UV/Vis absorption and PL spectroscopy (Figures 3d and S7e). The UV/Vis spectrum shows that the sheets are semiconducting and the corresponding optical band gap (E_g) is estimated to be 2.48 eV. A characteristic peak in the

PL spectrum was observed at 498 nm (phonon energy of 2.49 eV), which is in excellent agreement with the absorption spectrum (Figure 3d). For comparison, distinct characteristic peaks were observed in bulk boron and $NaBH_4$ (Figure S7f).

To gain further insight into the electronic properties of α' -4H-borophene, first-principles calculations based on the PBE0 hybrid exchange–correlation functional were performed. It was found that borophene is an indirect-band-gap semiconductor with a band gap of 2.04 eV at the Γ point between the valence-band maximum and the conduction-band minimum (Figures 3e and S14), and the corresponding projected density of states (DOS) is shown in Figure 3f. Additionally, the photon-absorption spectrum of borophene was calculated by first-principles calculations. The onset energy was observed at 2.5 eV in the xy plane and z direction, which is well consistent with the direct photon absorption at the Γ point in the Brillouin zone (red arrow, Figure 3e). The absorption exhibits a large similarity to that of reported boron hydride and ultrathin MoS_2 sheets.^[14, 22]

To reveal the growth mechanism of α' -4H-borophenes, we investigated the effect of the annealing temperature and reaction duration on the resulting products. Previous experiments have indicated that the release of hydrogen gas from $NaBH_4$ begins to rapidly accelerate at 450–500 °C.^[23] No products were obtained when the temperature was directly heated up to 500 °C, which is due to the absence of the B–B intermediate with a metastable structure for the rapid thermal decomposition of $NaBH_4$. In contrast, the annealing temperature of 490 °C is a suitable temperature for keeping the system stable and a prolonging duration up to 2 h is necessary to obtain the intermediate with high yield (Step I). Furthermore, the annealing temperature has to be raised to improve the crystallinity of the borophenes. It was found that the gas pressure in the system is raised drastically at a temperature of 550 °C, which is consistent with the thermoanalytical curve (Figure S9b). It is necessary to keep the annealing temperature at 550 °C for 30 min to prevent the intermediate product from being carried away by the hydrogen-gas stream and to further increase the yield of the target product (Step II). After that, the temperature was raised and kept at 600 °C for 30 min to produce the ultrastable borophenes with high crystallinity (Step III). Theoretically, the adsorption of alkali-metal atoms (Li, Na, and K) onto the boron sheet markedly increases the hydrogen-binding energy to form stable borophenes.^[24] Hence, the formation of the borophenes can be reasonably ascribed to the self-catalyzing growth of the metal Na acting as an in-situ gas template produced during the thermal decomposition of $NaBH_4$. It is well documented that $NaBH_4$ begins to decompose into NaH at 200 °C, after which NaH decomposes into Na and H_2 at higher temperatures of over 425 °C.^[25] Generally, the decomposition of $NaBH_4$ is summarized as follows:^[23, 25]



We also explored the influence of temperature on the quality of the borophenes in the range from 400 to 500 °C for

30 min reaction duration within intervals of 25 °C. All samples were dispersed into a 1 mol L⁻¹ HCl solution and no product was obtained at temperatures below 450 °C, while a small amount of gray solid was collected at 475 and 500 °C. Thick samples were produced at temperatures of above/below 600 °C (Figure S15), and the crystallinity of the samples tends to be amorphous due to the slow/rapid growth rate, respectively (Figure S16). Hence, the temperature of 600 °C is suitable to form borophenes with good crystallinity. Furthermore, it was also found that some samples are amorphous, which results from the structural destruction of the borophenes under high-energy electron irradiation for low-mass boron and hydrogen atoms,^[26] as shown in Figure S2e–i. The growth procedure of the borophenes is illustrated in Figure S17. The dynamics of forming the sheets was also probed at 600 °C. It was observed that the quality of the sheets was relatively weak after a reaction duration of 15 min (Figure S18a), while thicker sheets were produced for a reaction duration of over 30 min (Figure S18b–d). Therefore, a duration of 30 min is the optimal condition to synthesize the borophenes at 600 °C.

Based on their good stability and dispersibility in various solvents such as water and ethanol, the borophenes have great potential in borophene-based nanodevices. We selected them as the active layers and PVP polymers as insulators to fabricate a borophene-based memory device (Figure 4a),

which is similar to phosphene, graphene, and MoS₂ devices.^[27] A typical device exhibits an electrically bistable behavior (Figure 4b; scanning direction indicated by the arrow). The bipolar resistive-switching behavior was observed between the high-resistance state (HRS, OFF state) and the low-resistance state (LRS, ON state). The initial voltage was swept from 0 to -1 V and the current increased dramatically at a V_{set} of -0.33 V (Step 1). The transition from the HRS to the LRS is equivalent to a writing process in digital memory, and the device stays in the LRS within a voltage range from -1 to 0 V (Step 2). Additionally, the positive voltage was swept from 0 to +1 V, and the device continued to remain in the LRS state (Step 3). Another transition from the LRS to the HRS occurred with a V_{reset} of +0.53 V for the final voltage sweeping from +1 to 0 V (Step 4), which corresponds to the erasing process of the digital memory. The subsequent negative and positive sweeps suggest that the device can be re-written and re-erased, indicating a promising potential of borophene in advanced memory devices. The long-term stability of the device as a function of the operation time is shown in Figure 4c. No obvious current fluctuation was observed during the retention time of 600 s, and the device maintains an ON/OFF current of more than 3.0×10^3 at a reading voltage of 0.2 V, indicating its good stability.

To reveal the conduction mechanism of the borophene-based device, the typical I - V characteristics were assessed, as shown in Figure 4d. Region A and B are located in the OFF state, and the plot of $\ln(I)$ vs. $V^{1/2}$ from 0 to -0.12 V (region A) can be fitted to a straight line (inset in Figure 4e). Because borophenes dispersed in PVP can be regarded as trapping centers, the traps are occupied in the low-voltage regime (Figure S19a). Such a linear characteristic indicates that the conduction mechanism can be ascribed to thermionic emission,^[25–27] which arises from the low injection efficiency in the presence of the large barrier between the electrodes and the active borophene-PVP layer. For the low-conductance state with a voltage from -0.12 to -0.35 V, the charge-transport behavior is well consistent with the trap-controlled space-charge-limited conduction (SCLC) model. During the process, charges are transferred from PVP to the borophenes (Figure S19b) and then trapped by the sheets due to their lower energy level in comparison with PVP. Following the SCLC model, a free-carrier density that is lower than the trap density is induced by the borophenes. A transition region B is then reached, where the current increases non-linearly with a quadratic voltage dependence ($I \propto V^2$), and the slope increases to 2.09. In this region, the traps are completely filled with the increase of the applied voltage and a higher electron concentration is induced in the active layers of the device (Figure S19c). In region C, injected carriers in the active layers increase

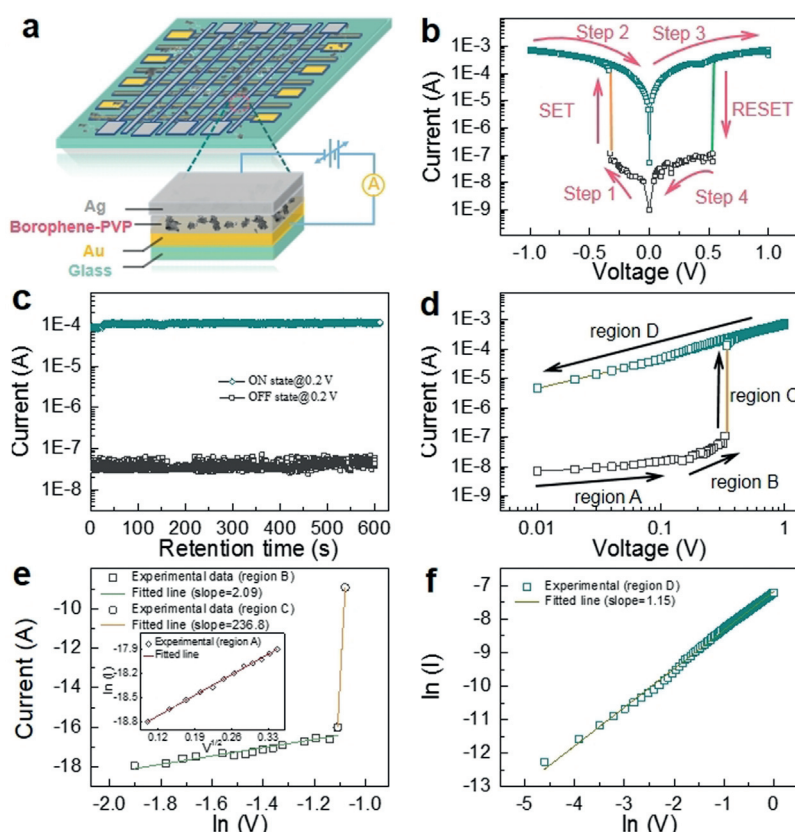


Figure 4. a) Schematic illustration of the Au/borophene-PVP/Ag/glass device. b) Current-voltage (I - V) curve of the device. c) Retention characteristic of the device in ON and OFF states at a reading voltage of 0.2 V. d) I - V characteristics of the device during the negative sweep. e), f) Linear fitting of the I - V curve in the OFF and ON states.

exponentially as the voltage rises close to the operating voltage, and conductive paths are formed in the active layers due to the higher electron concentration (Figure S19d). Accordingly, the formation of the conductive paths switches the device from the HRS to the LRS. Hence, an internal electric field is formed due to the loss of electrons accumulated in the active layer.

In contrary, the I - V relationship in the ON state (region D, Figure 4 f) exhibits an ohmic conduction behavior with a slope of around 1.15, indicating the formation of filament paths in the device during the single-electron-transfer (SET) process. Furthermore, trapped charges in the borophenes are not discharged after the device is powered off because of the insulating nature of the PVP material, which makes the device have a high conductivity and non-volatility. When the electric field is applied reversely, the charges are easily neutralized or de-trapped (Figure S19 a). The process results in the disappearance of the internal electric field. Consequently, the device returns to the HRS after a complete cycle, and the erasing process of the data storage continues to be executed. We have also compared the performance of reported nanomaterials such as C_{60} , MoS_2 , graphene oxide, and black phosphorus quantum dots (Table S3).^[27] The results suggest that the borophene device has an ultralow switching voltage of down to 0.35 V, demonstrating that it has potential applications in advanced memory devices with low energy consumption.

In summary, we have successfully prepared ultrastable crystalline semiconducting hydrogenated borophenes by an in-situ and three-step thermal-decomposition process. The obtained borophene is a novel 2D material with a $B_{1/9}$ structure and shows robust stability in strong acid and base solvents. Furthermore, the measured optical band gap of the borophene is in good agreement with that of first-principles calculations. Finally, a borophene-based memory device was fabricated to demonstrate a high-performance device application.

Acknowledgements

This work was supported by the National Natural Science Foundation of China (61774085), Six Talent Peaks Project in Jiangsu Province (XCL-046), the Fundamental Research Funds for the Central Universities (NE2017101), and the Priority Academic Program Development of Jiangsu Higher Education Institutions. The authors also thank Prof. C. Li for valuable help with the DFT calculations.

Conflict of interest

The authors declare no conflict of interest.

Keywords: boron · chemical vapor deposition · hydrogenation · monolayers · thin films

- [1] a) Z. A. Piazza, H. S. Hu, W. L. Li, Y. F. Zhao, J. Li, L. S. Wang, *Nat. Commun.* **2014**, *5*, 3113; b) H. J. Zhai, B. Kiran, J. Li, L. S. Wang, *Nat. Mater.* **2003**, *2*, 827–833; c) W. L. Li, X. Chen, T. Jian, T. T. Chen, J. Li, L. S. Wang, *Nat. Rev. Chem.* **2017**, *1*, 0071; d) A. P. Sergeeva, I. A. Popov, Z. A. Piazza, W. L. Li, C. Romanescu, L. S. Wang, A. I. Boldyrev, *Acc. Chem. Res.* **2014**, *47*, 1349–1358; e) L. S. Wang, *Int. Rev. Phys. Chem.* **2016**, *35*, 69–142.
- [2] A. J. Mannix, X. F. Zhou, B. Kiraly, J. D. Wood, D. Alducin, B. D. Myers, X. Liu, B. L. Fisher, U. Santiago, J. R. Guest, M. J. Yacaman, A. Ponce, A. R. Oganov, M. C. Hersam, N. P. Guisinger, *Science* **2015**, *350*, 1513–1516.
- [3] B. Feng, J. Zhang, Q. Zhong, W. Li, S. Li, H. Li, P. Cheng, S. Meng, L. Chen, K. Wu, *Nat. Chem.* **2016**, *8*, 563–568.
- [4] G. Tai, T. Hu, Y. Zhou, X. Wang, J. Kong, T. Zeng, Y. You, Q. Wang, *Angew. Chem. Int. Ed.* **2015**, *54*, 15473–15477; *Angew. Chem.* **2015**, *127*, 15693–15697.
- [5] a) S. Y. Xie, Y. Wang, X. B. Li, *Adv. Mater.* **2019**, *31*, 1900392; b) A. J. Mannix, Z. Zhang, N. P. Guisinger, B. I. Yakobson, M. C. Hersam, *Nat. Nanotechnol.* **2018**, *13*, 444–450; c) Z. Zhang, E. S. Penev, B. I. Yakobson, *Chem. Soc. Rev.* **2017**, *46*, 6746–6763.
- [6] a) Z. Zhang, E. S. Penev, B. I. Yakobson, *Nat. Chem.* **2016**, *8*, 525–527; b) X. Sun, X. Liu, J. Yin, J. Yu, Y. Li, Y. Hang, X. Zhou, M. Yu, J. Li, G. Tai, W. Guo, *Adv. Funct. Mater.* **2017**, *27*, 1603300.
- [7] a) X. Wu, J. Dai, Y. Zhao, Z. Zhuo, J. Yang, X. C. Zeng, *ACS Nano* **2012**, *6*, 7443–7453; b) Y. Liu, E. S. Penev, B. I. Yakobson, *Angew. Chem. Int. Ed.* **2013**, *52*, 3156–3159; *Angew. Chem.* **2013**, *125*, 3238–3241; c) Z. Zhang, Y. Yang, G. Gao, B. I. Yakobson, *Angew. Chem. Int. Ed.* **2015**, *54*, 13022–13026; *Angew. Chem.* **2015**, *127*, 13214–13218; d) E. S. Penev, S. Bhowmick, A. Sadrzadeh, B. I. Yakobson, *Nano Lett.* **2012**, *12*, 2441–2445.
- [8] R. Wu, I. K. Drozdov, S. Eltinge, P. Zahl, S. Ismail-Beigi, I. Božović, A. Gozar, *Nat. Nanotechnol.* **2019**, *14*, 44–49.
- [9] B. Kiraly, X. Liu, L. Wang, Z. Zhang, A. J. Mannix, B. L. Fisher, B. I. Yakobson, M. C. Hersam, N. P. J. A. N. Guisinger, *ACS Nano* **2019**, *13*, 3816–3822.
- [10] a) D. C. Elias, R. R. Nair, T. M. G. Mohiuddin, S. V. Morozov, P. Blake, M. P. Halsall, A. C. Ferrari, D. W. Boukhvalov, M. I. Katsnelson, A. K. Geim, K. S. Novoselov, *Science* **2009**, *323*, 610–613; b) R. Balog, B. Jørgensen, L. Nilsson, M. Andersen, E. Rienks, M. Bianchi, M. Fanetti, E. Lægsgaard, A. Baraldi, S. Lizzit, Z. Slijivancanin, F. Besenbacher, B. Hammer, T. G. Pedersen, P. Hofmann, L. Hornekær, *Nat. Mater.* **2010**, *9*, 315–319; c) M. Pumera, C. H. A. Wong, *Chem. Soc. Rev.* **2013**, *42*, 5987–5995; d) H. Liu, J. Gao, J. Zhao, *J. Phys. Chem. C* **2013**, *117*, 10353–10359; e) E. Bianco, S. Butler, S. Jiang, O. D. Restrepo, W. Windl, J. E. Goldberger, *ACS Nano* **2013**, *7*, 4414–4421.
- [11] a) Y. Jiao, F. Ma, J. Bell, A. Bilic, A. Du, *Angew. Chem. Int. Ed.* **2016**, *55*, 10292–10295; *Angew. Chem.* **2016**, *128*, 10448–10451; b) L. Kou, Y. Ma, C. Tang, Z. Sun, A. Du, C. Chen, *Nano Lett.* **2016**, *16*, 7910–7914; c) L. C. Xu, A. Du, L. Kou, *Phys. Chem. Chem. Phys.* **2016**, *18*, 27284–27289; d) L. Shao, X. Duan, Y. Li, Q. Yuan, B. Gao, H. Ye, P. Ding, *Phys. Chem. Chem. Phys.* **2019**, *21*, 7630–7634; e) B. Mortazavi, M. Makaremi, M. Shahrokhi, M. Raeisi, C. V. Singh, T. Rabczuk, L. F. C. Pereira, *Nanoscale* **2018**, *10*, 3759–3768; f) D. Li, J. He, G. Ding, Q. Tang, Y. Ying, J. He, C. Zhong, Y. Liu, C. Feng, Q. Sun, H. Zhou, P. Zhou, G. Zhang, *Adv. Funct. Mater.* **2018**, *28*, 1801685.
- [12] Z. Wang, T. Y. Lü, H. Q. Wang, Y. P. Feng, J. C. Zheng, *Phys. Chem. Chem. Phys.* **2016**, *18*, 31424–31430.
- [13] W. H. Eberhardt, B. Crawford, W. N. Lipscomb, *J. Chem. Phys.* **1954**, *22*, 989–1001.

- [14] a) H. Nishino, T. Fujita, N. T. Cuong, S. Tominaka, M. Miyauchi, S. Iimura, A. Hirata, N. Umezawa, S. Okada, E. Nishibori, A. Fujino, T. Fujimori, S. i. Ito, J. Nakamura, H. Hosono, T. Kondo, *J. Am. Chem. Soc.* **2017**, *139*, 13761–13769; b) R. Kawamura, N. T. Cuong, T. Fujita, R. Ishibiki, T. Hirabayashi, A. Yamaguchi, I. Matsuda, S. Okada, T. Kondo, M. Miyauchi, *Nat. Commun.* **2019**, *10*, 4880.
- [15] H. Tang, S. Ismail-Beigi, *Phys. Rev. Lett.* **2007**, *99*, 115501.
- [16] H. Werheit, V. Filipov, U. Kuhlmann, U. Schwarz, M. Armbrüster, A. Leithe-Jasper, T. Tanaka, I. Higashi, T. Lundström, V. N. Gurin, M. M. Korsukova, *Sci. Technol. Adv. Mater.* **2010**, *11*, 023001.
- [17] a) S. L. Chou, J. I. Lo, Y. C. Peng, M.-Y. Lin, H. C. Lu, B. M. Cheng, J. F. Ogilvie, *Chem. Sci.* **2015**, *6*, 6872–6877; b) W. C. Price, *Sci. Technol. Adv.* **1948**, *16*, 894–902.
- [18] G. Parakhonskiy, V. Vtech, N. Dubrovinskaia, R. Caracas, L. Dubrovinsky, *Solid State Commun.* **2013**, *154*, 34–39.
- [19] S. Nakano, R. J. Hemley, E. A. Gregoryanz, A. F. Goncharov, H. K. Mao, *J. Phys. Condens. Matter* **2002**, *14*, 10453–10456.
- [20] N. J. Hess, M. E. Bowden, V. M. Parvanov, C. Mundy, S. M. Kathmann, G. K. Schenter, T. Autrey, *J. Chem. Phys.* **2008**, *128*, 034508.
- [21] a) R. Rao, A. E. Islam, P. M. Campbell, E. M. Vogel, B. Maruyama, *2D Mater.* **2017**, *4*, 025058; b) Y. Zhao, H. Wang, H. Huang, Q. Xiao, Y. Xu, Z. Guo, H. Xie, J. Shao, Z. Sun, W. Han, X. F. Yu, P. Li, P. K. Chu, *Angew. Chem. Int. Ed.* **2016**, *55*, 5003–5007; *Angew. Chem.* **2016**, *128*, 5087–5091.
- [22] A. Splendiani, L. Sun, Y. Zhang, T. Li, J. Kim, C. Y. Chim, G. Galli, F. Wang, *Nano Lett.* **2010**, *10*, 1271–1275.
- [23] W. Grochala, P. P. Edwards, *Chem. Rev.* **2004**, *104*, 1283–1316.
- [24] S. Er, G. A. de Wijs, G. Brocks, *J. Phys. Chem. C* **2009**, *113*, 18962–18967.
- [25] P. Martelli, R. Caputo, A. Remhof, P. Mauron, A. Borgschulte, A. Züttel, *J. Phys. Chem. C* **2010**, *114*, 7173–7177.
- [26] R. Arenal, A. Lopez-Bezanilla, *ACS Nano* **2014**, *8*, 8419–8425.
- [27] a) X. Zhang, H. Xie, Z. Liu, C. Tan, Z. Luo, H. Li, J. Lin, L. Sun, W. Chen, Z. Xu, L. Xie, W. Huang, H. Zhang, *Angew. Chem. Int. Ed.* **2015**, *54*, 3653–3657; *Angew. Chem.* **2015**, *127*, 3724–3728; b) X. D. Zhuang, Y. Chen, G. Liu, P. P. Li, C. X. Zhu, E. T. Kang, K. G. Noeh, B. Zhang, J. H. Zhu, Y. X. Li, *Adv. Mater.* **2010**, *22*, 1731–1735; c) J. Liu, Z. Zeng, X. Cao, G. Lu, L. H. Wang, Q. L. Fan, W. Huang, H. Zhang, *Small* **2012**, *8*, 3517–3522; d) S. Paul, A. Kanwal, M. Chhowalla, *Nanotechnology* **2006**, *17*, 145.

Manuscript received: January 20, 2020

Revised manuscript received: March 19, 2020

Accepted manuscript online: April 3, 2020

Version of record online: May 8, 2020